Effect of mesa geometry on low-terahertz frequency range plasmons in two-dimensional electron systems

A. Dawood

Imperial College London, London SW7 2AZ, UK

S. J. Park, R. Parker-Jervis, C. D. Wood, L. Li, E. H. Linfield, A. G. Davies, J. E. Cunningham

University of Leeds, Woodhouse Lane, Leeds, LS2 9JT, UK

O. Sydoruk

Imperial College London, London SW7 2AZ, UK

E-mail: osydoruk@imperial.ac.uk

Abstract. We demonstrate engineering of the low-terahertz range plasmonic spectra of two-dimensional electron systems by modifying their geometry. Specifically, we have modelled, fabricated, and measured two devices for comparison. The first device has a rectangular channel, while the second is trapezoidal, designed to support a richer plasmonic spectrum by causing variation in the device width along the direction of plasmon propagation. We show that while plasmon resonant frequencies and field distributions in the rectangular device can largely be described by a simple one-dimensional analytical model, the field distributions modelled in the trapezoidal device shows a more complex pattern with significant variation along the length of the channel, so requiring a two-dimensional treatment. The results illustrate the potential of modifying the channel geometry to obtain different spectra in experiments, with potential applications in the design of novel terahertz-range devices, such as plasmon-based sources and detectors.

PACS numbers: 73.20.Mf, 07.57.Hm, 84.30.Le, 84.30.Ng

Submitted to: *J. Phys. D: Appl. Phys.*

1. Introduction

Two-dimensional (2D) plasmons are attracting significant attention both as a tool to study physical properties of novel materials [1, 2, 3, 4] and owing to their potential use in devices. The lack of widely available compact, powerful, efficient, and cheap terahertz (THz) sources makes applications of 2D plasmons in THz generation particularly attractive. In a seminal paper [5], Dyakonov and Shur predicted that plasmons propagating in the channel of a field-effect transistor may become unstable when a dc current flows in the channel. Other effects considered for potential THz sources include transit-time [6, 7] as well as travelling-wave- and Cherenkov-type instabilities [8, 9, 10]. Recent studies on electrically-driven plasmon sources have concentrated on, for example, emission by Dirac electrons [11], instability at high electric fields [12], channels of variable width [13], and electromagnetic modelling [14].

2D plasmons have also found applications in THz detectors. Nonresonant (e.g. [15]) and resonant (e.g. [16]) detection, as well as single-[17] and multi-pixel [18] imaging were demonstrated in high-mobility electron transistors. Terahertz detectors based on graphene have also been realised [19, 20].

The geometry of a channel supporting plasmons is an important factor determining its frequency response. Ever since the first observation of 2D plasmons in a semiconductor heterostructure [21], the most widely used channel geometry has been that of a rectangle. Rectangular channels have been combined both with grating couplers for plasmon excitation by free-space radiation [21, 22, 23, 24, 25, 26] and with gates for electrostatic control of the charge density [27, 24, 28]. They can also be readily connected to Ohmic contacts, antennas [29, 30], and waveguides [31, 32, 33]. A geometry with a rectangular channel is shown schematically in figure 1(a), while a micrograph of a fabricated device is shown in figure 1(b). The channel is connected, via Ohmic contacts, to the central conductors of two coplanar waveguides. One waveguide is used for in- and the other for out-coupling of THz signals. A metallic gate is formed over a portion of the channel, and a dc voltage applied to it changes the electron density in the channel underneath, allowing the plasmon wavelength to be controlled. If one dimension of a rectangular channel is much larger than the other, any variation in plasmons along the longer dimension can be ignored. This simplifying assumption has underpinned the majority of theoretical studies, from the classical derivations of plasmon dispersion relations [34, 21, 22] to analyses of plasmonic sources [5, 35, 36, 37] and detectors [38, 7, 39].

Although less common, disk-shaped 2D channels have also been used to study bulk and edge magnetoplasmons [40, 41] and, more recently for example, to observe retardation effects [42, 43] as well as low-loss plasmon modes [44]. A related geometry is the Corbino field-effect transistor, which has cylindrical source, drain, channel, and gate, that was shown [45] to enable plasmon instability in the presence of a dc current. Although cylindrical symmetry of such geometries often simplifies analysis, practical difficulties of establishing electrical connection to the terminals make them less attractive

for device applications.

Plasmonic effects caused by lateral variations of the channel geometry present a hitherto relatively unexplored area with potential for device applications. Two recent studies [46, 13] predicted that lateral variations in the geometry of a rectangular channel may lead to plasmon instabilities. In this paper, in addition to the rectangular device geometry of figure 1(a), we discuss a novel device with trapezoidal geometry shown schematically in figure 1(b). A micrograph of a fabricated device is shown in figure 1(d). There are several reasons for choosing the trapezoidal shape. First, the trapezoidal device of figures 1(b) and (d) differs from the rectangular device of figures 1(a) and (c) only in one parameter (namely, the channel geometry) allowing for a direct comparison between the two geometries. Second, in contrast to a disk geometry, the trapezoidal shape permits simple electrical access the gate and ohmic contacts. Third, the non-constant width of a trapezoidal channel can be expected to create plasmon resonant modes that vary along both dimensions yielding a denser spectrum than that observed in the rectangular channel. Finally, the trapezoidal device might potentially be used to study plasmon gain in an electrically-driven configuration, since the electron drift velocity varies along the channel length.

Section 2 presents a theoretical analysis of the two device geometries. Section 3 presents their experimental investigation and compares the results to our theoretical predictions. Section 4 draws conclusions.

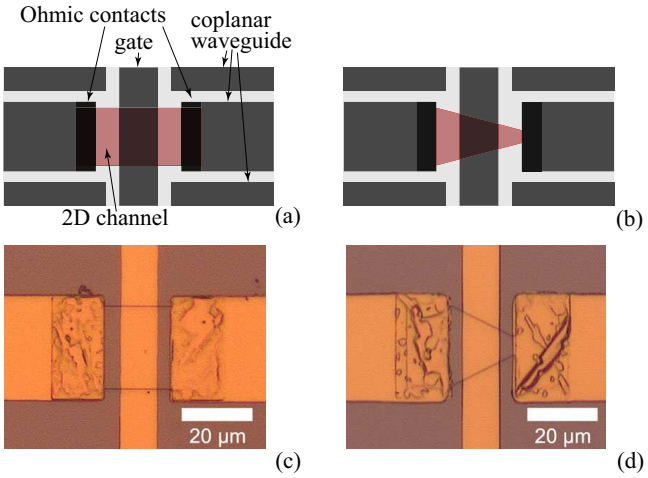

Figure 1. Schematic presentations of device geometries, (a) and (b), and micrographs of fabricated devices, (c) and (d). The standard geometry, (a) and (c), comprises a rectangular channel connected, via Ohmic contacts, to two coplanar waveguides. The metallic gate formed over a portion of the channel is used for electrostatic control of the electron density underneath. The novel geometry, (b) and (d), comprises a trapezoidal channel, whose width varies along the propagation direction.

Table 1. Dimensions used in simulations (see figure 2).

length of 2D channel, l	18.8 μm
width of 2D channel, w	23.4 μm
coplanar waveguide width of centre conductor, w_C	30 μm
AlGaAs mesa height, h	125 nm
depth of 2D channel beneath the gate, d	75 nm
length of first ungated 2D channel section, l_{s1}	4 μm
length of second ungated 2D channel section, l_{s2}	4 μm
gate width/length of gated 2D channel section, l_g	10.8 μm
length of ohmic contact longitudinal extension, l_e	4 μm
coplanar waveguide gap, w_g	20 μm
width of waveguide ground plane, w_G	15 μm
substrate thickness, t	30 μm
depth of ohmic contact, t_c	1250 nm
length of ohmic contact, l_c	12.5 μm
length of coplanar waveguide feed sections, l_{wg}	75 μm
length of PML sections, l_{PML}	37.5 μm

2. Theory

This section presents an analytical and numerical investigation of the plasmon spectra in the two devices shown in figure 1. To provide a background and to introduce our methodology, we first discuss, in section 2.1, the device with the traditional rectangular channel, see figure 1(a). In section 2.2 we discuss trapezoidal channel geometry (figure 1(b)).

2.1. Device with rectangular channel

Figure 2 shows schematically both top and side views of the rectangular device, with dimensions summarised in table 1. The channel is formed within a rectangular mesa on a substrate comprising a GaAs/AlGaAs heterostructure [31]. A rectangular gate is laid over the 2D channel, leaving two short ungated sections on either side. The channel is terminated by Ohmic contacts at both ends, and these are connected to the central conductors of two coplanar waveguides. The substrate material is GaAs with a relative permittivity of 12.4. The mesa material is AlGaAs with a relative permittivity of 11.5. The charge carriers in the channel are electrons with an effective electron mass of $m = 0.067m_0$, where m_0 is the free electron mass. The electron density in the channel is $n_0 = 7.5 \times 10^{11}$ cm^{-2}. The electron density under the gate can be reduced by a dc voltage, and the junctions between the gated and ungated sections of the channel are assumed to be abrupt.

We analysed the structure in a commercial full-wave electromagnetic solver using the finite-element method. Signals were excited in the coplanar waveguides by one of four lumped-element ports placed between the central and the outer conductors [see figure 2(a)] and collected at the other ports. The waveguides were terminated by two

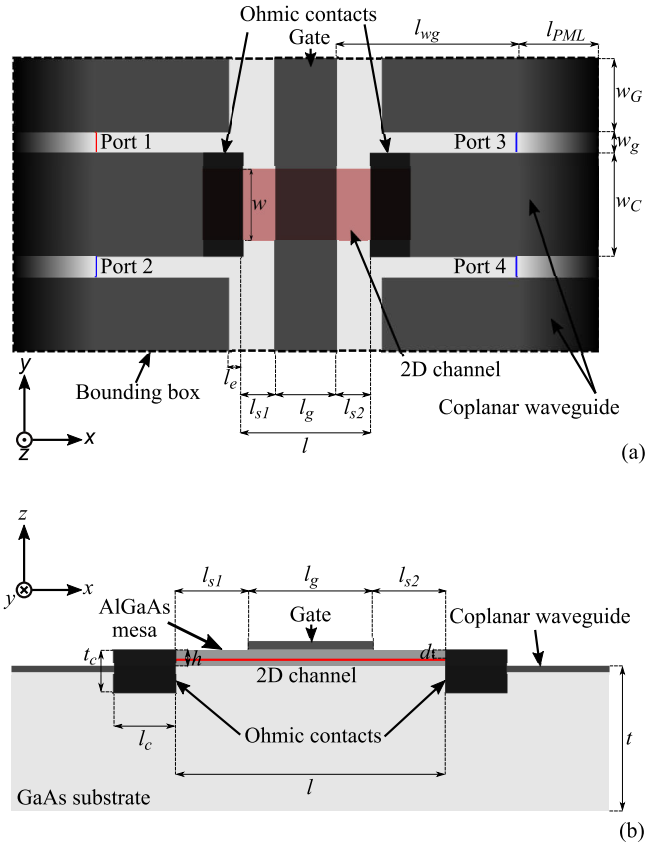

Figure 2. Detailed schematic presentation of a device with a rectangular 2D channel: (a) top-view (b) side-view.

perfectly-matched layers, and the entire geometry was enclosed in a perfectly conducting box with dimensions 240 μm $\times$ 130 μm $\times$ 60 μm. The electron motion was described by a damped Euler's equation, leading to the standard Drude form of the conductivity

$$\sigma = \frac{e^2 n_0}{j\omega\left(1 + \frac{1}{j\omega\tau}\right)} \tag{1}$$

where ω is the angular frequency, e is the electron charge, and τ is the relaxation time, taken as 7 ps. The dimensions, the electron density, and the relaxation time were chosen to correspond to the experiments (see section 3) and to allow direct comparison between the two geometries.

In the simulations, port 1 was excited between 30 and 400 GHz and signals transmitted through the device were collected at ports 2–4. The simulations were repeated for a range of values of the gated electron density between 7.5×10^{11} cm^{-2} and 3×10^{11} cm^{-2}. To emphasise plasmon resonances (and provide a link to the measurement technique, see section 3), figure 3 shows, as a colour map, the absolute value of the derivative of the transmission coefficient to port 4 with respect to the gated electron density, calculated as $|\Delta S_{41}(n_0)/\Delta n_0|$. A number of resonances can be seen whose frequencies depend on the electron density. At the resonant peaks corresponding to the

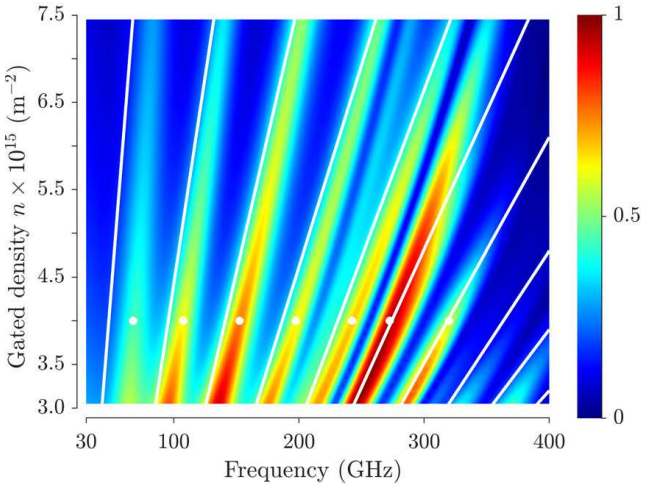

Figure 3. Simulated absolute value of the derivative of a transmission coefficient with respect to gated electron density (colour map) for the rectangular device. Analytically calculated resonant frequencies (white lines).

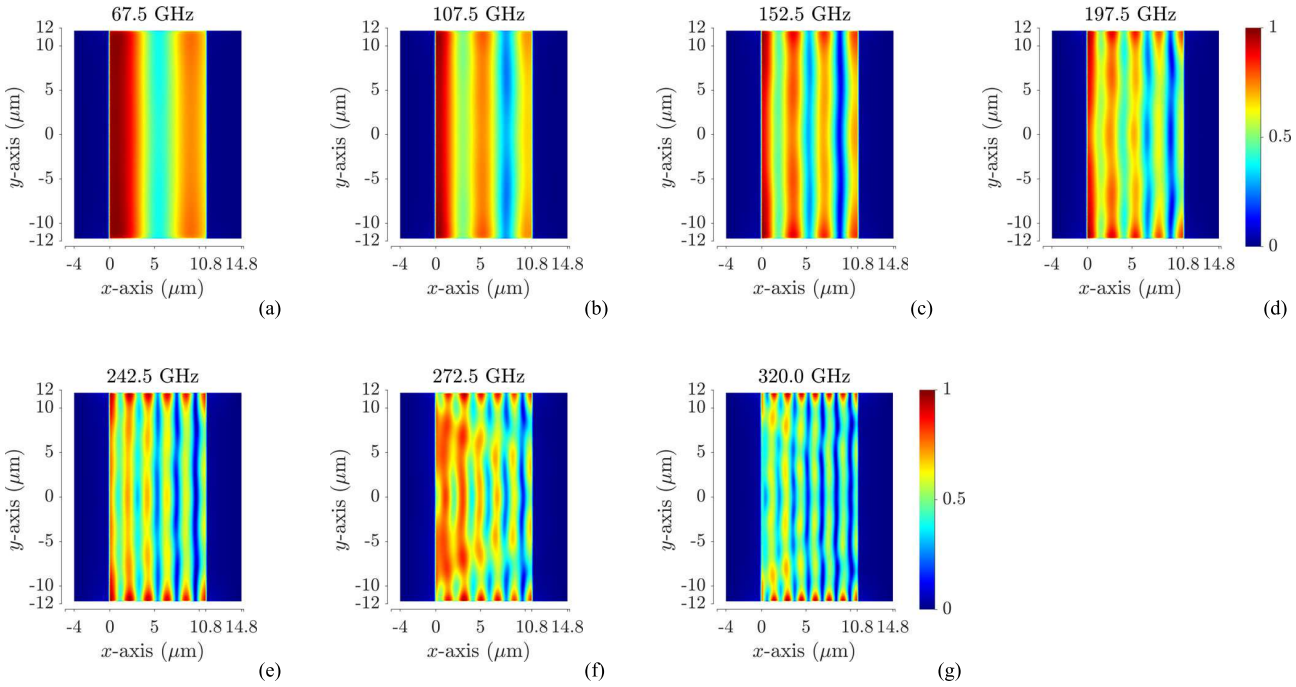

Figure 4. Absolute values of the E_z field component simulated for the rectangular device at resonant peaks shown by white circles in figure 3.

density of 4×10^{11} cm^{-2} (shown by white circles in figure 3), figure 4 shows colour maps of the absolute value of the E_z field component at the side of the channel that faces the gate, allowing the pattern of plasmons generated underneath the gate to be visualised.

The main aspects of the resonant behaviour can be explained using a basic model as follows. The well-known dispersion relation for gated plasmons has the following

form (ignoring collisions)

$$-\mathrm{j}\frac{e^2 n_0 q}{\varepsilon_0 \varepsilon_\mathrm{d} m\omega^2} = 1 + \mathrm{j}\cot(qd) \tag{2}$$

where q is the transverse plasmon wavenumber, and ε_d is the relative permittivity of the dielectric surrounding the channel. The transverse, q, and the longitudinal, k, wavenumbers obey the wave dispersion relation in the dielectric, which has the form

$$q^2 + k^2 = \varepsilon_\mathrm{d}\frac{\omega^2}{c^2} \tag{3}$$

where c is the free-space light velocity. Assuming that plasmons totally reflect at all four edges of the gated section of the channel, the longitudinal wavenumber will be quantised as

$$k = \pi\sqrt{\frac{M^2}{l_g^2} + \frac{N^2}{w^2}} \tag{4}$$

where M and N are integers. The white lines in figure 3 show the position of resonances calculated from (4) with $M = 1...9$ and $N = 0$. These are the resonances that are predicted by the one-dimensional model that ignores the finite width of the channel, and they agree well with all but one simulated resonances. The simulated resonance not predicted by (4) lies between the fourth and the fifth analytical resonances. It has a low amplitude and is likely to be a higher-order mode with $N > 0$. The field distributions for the lowest two resonances, shown in figures 4(a) and (b), further justify the use of the one-dimensional model, as they show little variation along the channel width. The field distribution for the third resonance ($M = 3$), figure 4(c), is still dominated by the $N = 0$ resonance but also shows evidence of resonances with $N > 0$ being excited. For $M = 3$, the analytically calculated resonant frequencies are 145 GHz for $N = 0$, 148 GHz for $N = 1$, and 150 GHz for $N = 2$. Because these values are close to each other, higher-order resonances ($N > 0$) may be excited simultaneously with the fundamental resonance ($N = 0$). However, the individual resonances with different values of N are not distinguishable in figure 3 owing to loss. Variation in the x-direction remains the prominent feature of the field distributions in figures 4(d)–(g), and each shows excitation of a resonance with increasing values of N. At the same time, these distributions show additional variation in the y-direction. All field amplitudes in figure 4 decrease from left to right. The structure is excited from the left coplanar waveguide, and signals decay in the lossy channel as they propagate to the right. Figures 4(d)–(g) also show increased field amplitudes along the top and bottom edges, suggesting excitation of edge plasmons [47, 48, 41] in addition to the bulk ones described by (2) and (4).

2.2. Device with trapezoidal channel

The trapezoidal channel (figure 1(b)), had a short base length of 5.1 μm, with all other parameters the same as in the rectangular geometry. The colour map in figure 5 shows the values of simulated derivative of transmission with respect to the gated density.

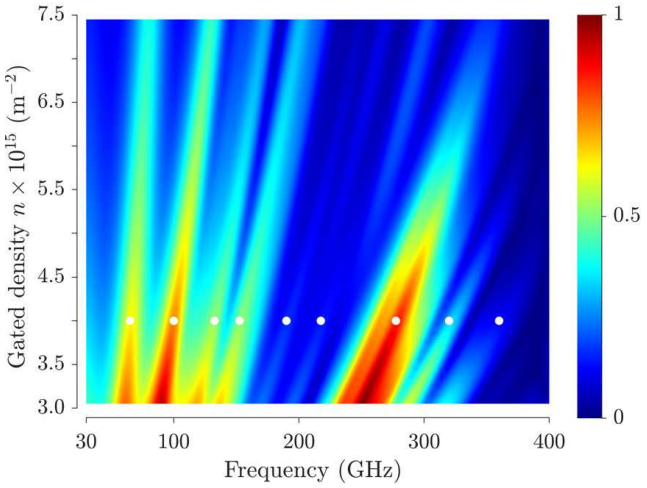

Figure 5. Simulated absolute value of the derivative of a transmission coefficient with respect to gated electron density (colour map) for the trapezoidal device.

There are four dominant resonances below 150 GHz. Above 150 GHz, there is a single broad area with high values of the derivative (which appears to be a combination of resonances), and several weaker resonances. Figure 6 shows field distributions simulated at the nine resonant peaks shown by white circles in figure 5. The resonances show pronounced variation of the amplitude both along and across the channel. As with the rectangular geometry, edge excitation is also present, especially at higher frequencies.

Comparing the simulation results for the rectangular and the trapezoidal devices, we can see that the trapezoidal device has a denser spectrum at the lower end of the simulated frequency range, with the associated advantage of observing more resonant modes in band-limited experiments. On the other hand, the rectangular device is expected to show higher amplitude signals (in the derivative of transmission coefficient with electron density) at the upper end of the spectrum. The trapezoidal device also has a more complex field distributions than the rectangular device, with additional strong variation of the fields along the channel width, as well as stronger edge excitations.

3. Experiment

We fabricated and measured the performance of two devices with the geometries shown in figures 1(a) and (b). Figures 1(c) and (d) show their micrographs. Fabrication and measurements followed the procedure detailed elsewhere [31, 32, 33]. The rectangular device comprised an 18.8-μm-long rectangular mesa. Three plasmonic cavities were defined by the two ungated cavities ($\sim$4 μm long), either side of one 10.8-μm-long gated cavity as shown in figure 1(c). The trapezoidal device comprised an 18.8-μm-long trapezoidal mesa. Three plasmonic cavities were defined by two ungated cavities ($\sim$4 μm long), either side of one 10.8-μm-long gated cavity as shown in figure 1(d).

In order to measure the frequency response of the fabricated devices, THz signals

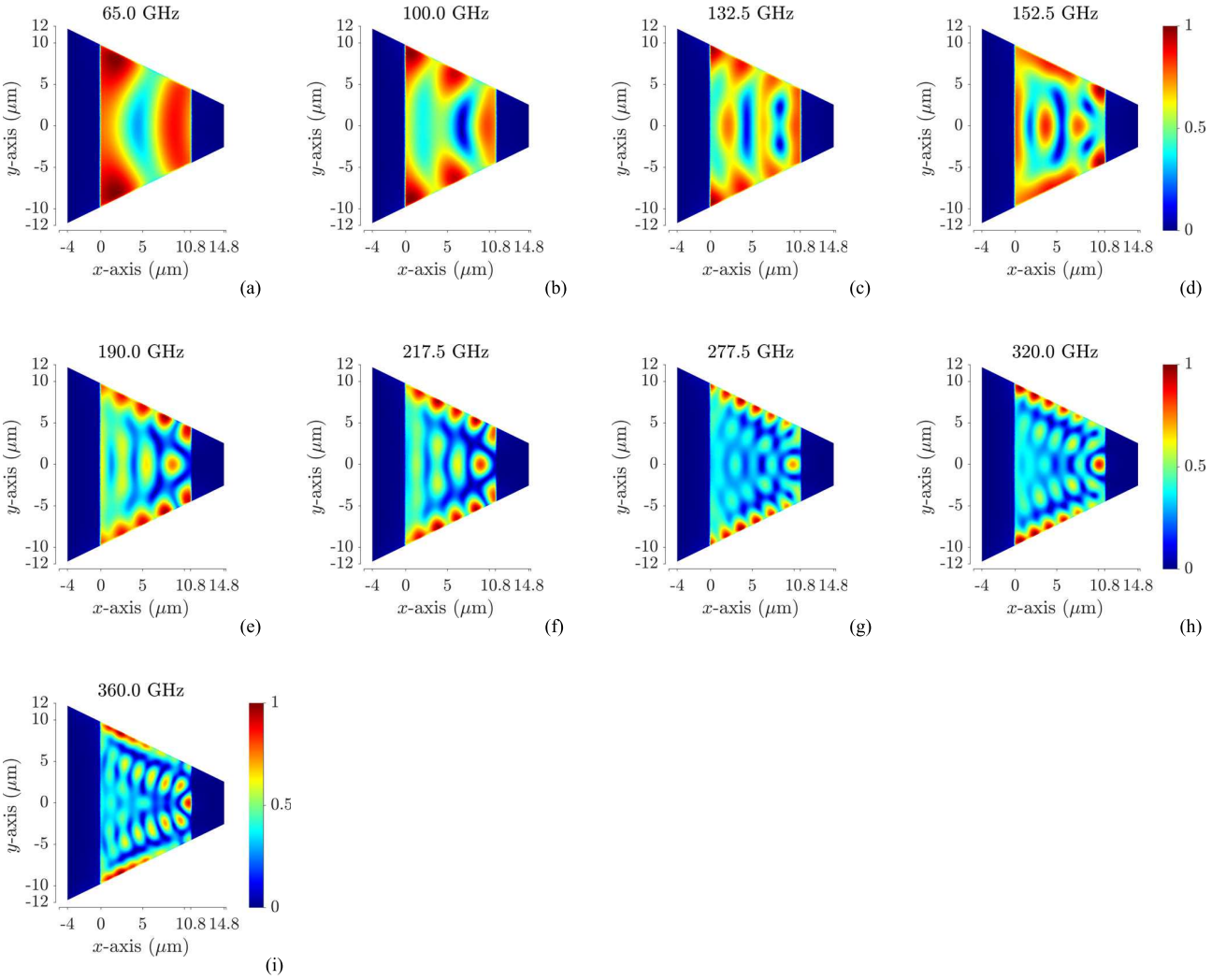

Figure 6. Absolute values of the E_z field component simulated for the trapezoidal device at resonant peaks shown by white circles in figure 5.

were generated by laser pulse excitation of one of the photoconductive switches, which was biased at 10 V dc and injected into a coplanar waveguide. The THz pulse transmitted through the channel was then detected at a switch on the other side. A gate-modulation technique was used to enhance the signal-to-noise ratio and to eliminate the background signal. An ac voltage of 100 mV RMS at 87 Hz was superimposed onto the gate bias allowing lock-in detection of the current pulses propagating through the gated mesa.

Figure 7(a) shows, as a colour map, the spectrum of the measured gate-modulation signals for the rectangular device at different gate voltages. Figure 7(c) shows the measured spectra for the trapezoidal device. The white dashed lines in both figures follow the resonant peaks; these were determined visually.

Since we performed simulations for varying electron density rather than gate voltage, a relationship between the two has to be known to enable direct comparisons.

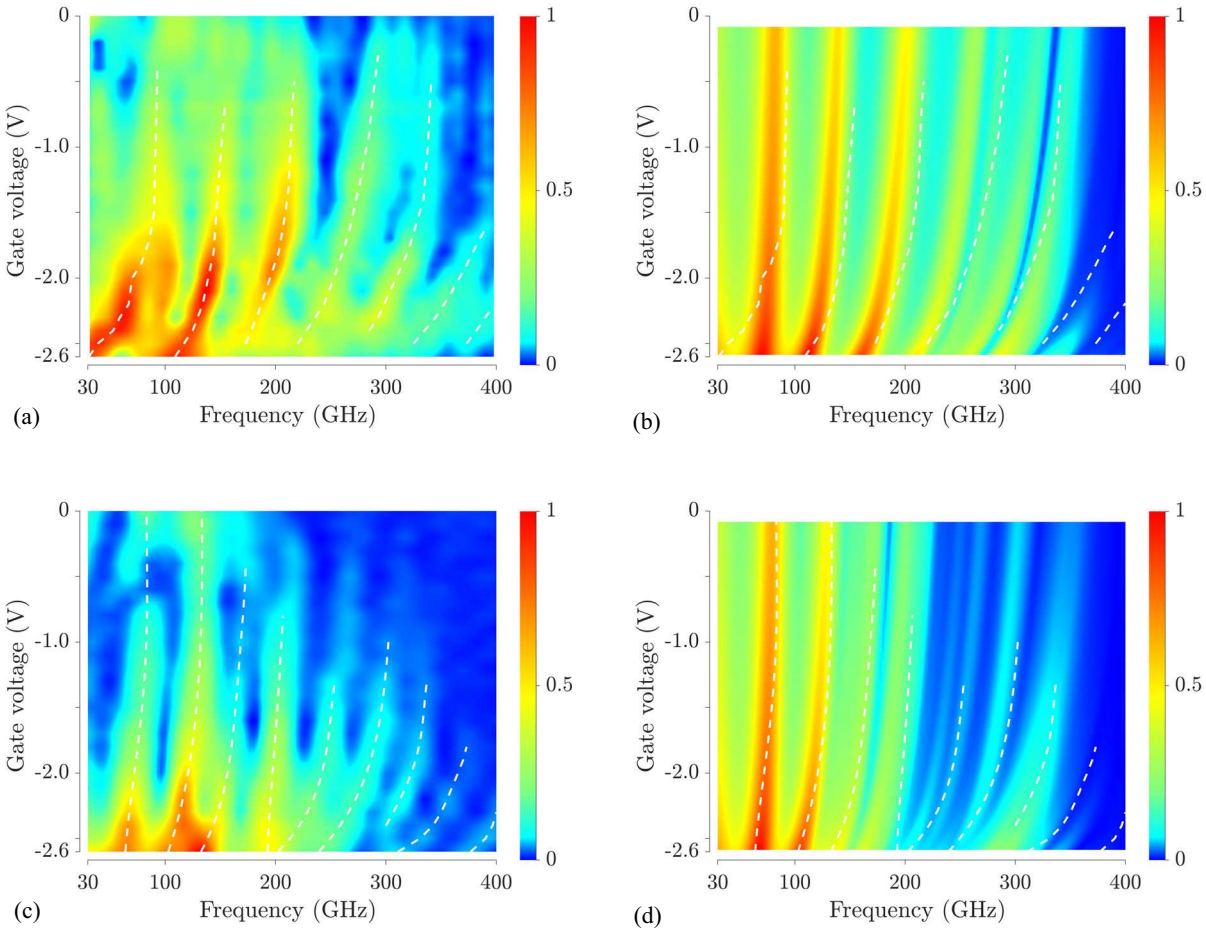

Figure 7. Measured (a) and simulated (b) gate-modulation signals for the rectangular device, and measured (c) and simulated (d) signals for the trapezoidal device. The dashed white lines show positions of the measured resonances.

However, a relationship between the gate voltage and the electron density could not be directly measured since the Shubnikov-De Haas oscillation signal from the gated region of the devices was weak, owing to the reduced overall size of the gated area compared to devices used in our previous work [31, 32, 33]. We have therefore taken a value of the density Shubnikov-De Haas oscillations observed in the ungated region, and then used the second experimental resonance of the trapezoidal device to fit a relationship for $n(V_g)$. The resulting empirical relationship was $n = 10^{15} \times (-0.06418V_g^4 - 0.14201V_g^3 - 0.16056V_g^2 + 0.5462V_g + 7.5)$, where V_g is in Volts and n is in m^{-2}.

In addition, we approximated the frequency content of the excitation pulses by assuming that the excitation amplitude decays exponentially with frequency f, as $\exp(-7.5f \times 10^{-12})$ [49]. Figure 7(b) shows the simulated resonances for the rectangular device, and figure 7(d) shows the resonances for the trapezoidal device. These resonances are the same as in figures 3 and 5, but with the vertical axis converted into gate voltage

and accounting for the decay of the excitation power with frequency. To aid comparison between the experiment and simulations, the same white dashed lines as in figures 7(a) and (c) are reproduced in figures 7(b) and (d).

For the rectangular device, compared to our previous experiments [33], we were able to observe more resonances, owing to shortened ungated portions of the channel that leads to smaller propagation loss. Seven resonances were observed, (see figure 7(a)), although those at higher frequencies are weak (owing to the decay of the excitation signal). Eight resonances are predicted by the simulations. For the first three resonances, the experimental frequencies are higher than the simulated ones, though these differences are of the order of the experimental frequency resolution. The fourth resonance is observed in a frequency region where simulations show two theoretical resonances. At larger negative voltages, the frequency of the measured resonance agrees with the frequency of the fourth simulated resonance, but it follows the fifth simulated resonance for smaller negative voltages. Likewise, the frequency of fifth measured resonance shifts from the sixth to the seventh simulated resonance as the gate voltage becomes less negative. Possibly, high experimental loss precludes observation of the separate simulated modes. The sixth experimental resonance, on the other hand, is blue-shifted relative to the closest (eighth) simulated one. There is no simulated resonance corresponding to the seventh experimental one, since its frequency lies outside the simulated range. The simulations reproduce qualitatively the main features of the strength of the measured signal. Both in the simulations and the measurements, the signals are highest at low voltages and low frequencies. The lowest frequencies have the strongest excitation signal. At the lowest voltages, on the other hand, the voltage swing due to gate modulation produces the largest change of the electron density, and therefore the largest variation of the transmission coefficient (which is the quantity we both measured and simulated).

For the trapezoidal device, nine resonances are observed experimentally (figure 7(c)). The positions of the measured and simulated resonances largely agree well with each other, and for every measured resonance a corresponding theoretical one can be identified. However, the simulations predict two closely spaced resonances between 200 and 250 GHz, whereas the measurements show a single resonance. It is probably because of the lower low frequency resolution in the experiment.

Comparison of the measured spectra of the rectangular and trapezoidal devices confirms the main aspects of the theoretical predictions. The trapezoidal device has a richer spectrum; in the experiment, we identified nine resonances between 30 and 400 GHz, whereas the rectangular device had seven. Below 150 GHz, the trapezoidal device showed four resonances against three in the rectangular device. However, the measured signals for the rectangular device are relatively stronger, across a wider range of gate voltages, for the upper end of the frequency range than they are for the trapezoidal device. Although field distributions were not directly measured, the simulated field patterns (see figures 4 and 6) offer a possible explanation. The strong variation of fields along the channel width in the trapezoidal device suggest that the plasmon velocity

along the channel is lower than in the rectangular device, leading to higher propagation loss.

4. Conclusions

The simulated resonances in the device with both channel and gate of a rectangular shape largely conformed to the predictions of a simple one-dimensional theory. The frequencies of the simulated resonances agreed well with those predicted from the plasmon dispersion relation, and the field distributions were dominated by variation along the channel length. However, transverse variation of the fields and excitation close to the channel edges became more apparent for the higher-frequency resonances, and point to simultaneous excitation of multiple resonant modes. The simulated resonant frequencies agreed well with the measurements.

The simulated field distributions for the trapezoidal device showed variation along both dimensions of the channel for all resonances, precluding the one-dimensional analysis to which the other device is amenable. However, both the simulated and measured spectra were richer than for the rectangular device, which suggests that the trapezoidal device is a more attractive choice for observing resonant behaviour in bandwidth-limited experiments.

An alternative to the trapezoidal device is one comprising a channel, a gate, and ohmic contacts of cylindrical shape. This geometry can be expected to exhibit properties similar to our trapezoidal device but, owing to its cylindrical symmetry, would permit an analytical treatment. Other alternative designs could implement relatively abrupt changes in the channel width, in contrast to the gradual variation in the trapezoidal device. It has already been predicted [13] that such devices could exhibit instabilities in the THz range.

Our results show that modifying the channel geometry provides a viable new route to engineer plasmon spectrum in devices that comprise two-dimensional materials, which will be useful for the design of novel plasmon-based devices in the terahertz range.

Acknowledgments

The authors gratefully acknowledge financial support provided by the EPSRC (grants EP/R004994/1, EP/R00501X/1, EP/P021859 and EP/V004743/1). The data that support the findings of this study are openly available at the following DOI: 10.14469/hpc/8792.

References

[1] L. Ju, B. Geng, J. Horng, C. Girit, M. Martin, Z. Hao, H. A. Bechtel, X. Liang, A. Zettl, Y. R. Shen, and F. Wang. Graphene plasmonics for tunable terahertz metamaterials. *Nature Nanotech.*, 6(10):630, 2011.

[2] A. N. Grigorenko, M. Polini, and K. S. Novoselov. Graphene plasmonics. *Nature Photon.*, 6(11):749–758, 2012.

[3] Z. Fei, A. S. Rodin, G. O. Andreev, W. Bao, A. S. McLeod, M. Wagner, L. M. Zhang, Z. Zhao, M. Thiemens, G. Dominguez, M. M. Fogler, A. H. Castro Neto, C. N. Lau, F. Keilmann, and D. N. Basov. Gate-tuning of graphene plasmons revealed by infrared nano-imaging. *Nature*, 487(7405):82–85, 2012.

[4] H. Yan, T. Low, W. Zhu, Y. Wu, M. Freitag, X. Li, F. Guinea, Ph. Avouris, and F. Xia. Damping pathways of mid-infrared plasmons in graphene nanostructures. *Nature Photon.*, 7(5):394–399, 2013.

[5] M. Dyakonov and M. Shur. Shallow water analogy for a ballistic field-effect transistor: new mechanism of plasma wave generation by a dc current. *Phys. Rev. Lett.*, 71:2465–2468, 1993.

[6] V. Ryzhii, A. Satou, and M. S. Shur. Plasma instability and terahertz generation in hemts due to electron transit-time effect. *IEICE Trans. on Electron.*, E89-C(7):1012–1019, 2006.

[7] V. Ryzhii, A. Satou, T. Otsuji, and M. S. Shur. Plasma mechanisms of resonant terahertz detection in a two-dimensional electron channel with split gates. *J. Appl. Phys.*, 103(1):014504, 2008.

[8] S. A. Mikhailov. Plasma instability and amplification of electromagnetic waves in low-dimensional electron systems. *Phys. Rev. B*, 58:1517–1532, 1998.

[9] S.M. Komirenko, K. W. Kim, V. A. Kochelap, I. Fedorov, and M. A. Stroscio. Coherent optical phonon generation by the electric current in quantum wells. *Appl. Phys. Lett.*, 77(25):4178–4180, 2000.

[10] O. Sydoruk, V. Kalinin, and L. Solymar. Terahertz instability of optical phonons interacting with plasmons in two-dimensional electron channels. *Appl. Phys. Lett.*, 97:062107–1–3, 2010.

[11] D. Svintsov. Emission of plasmons by drifting dirac electrons: A hallmark of hydrodynamic transport. *Phys. Rev. B*, 100(19):195428, 2019.

[12] V. V. Korotyeyev and V. A. Kochelap. Plasma wave oscillations in a nonequilibrium two-dimensional electron gas: Electric field induced plasmon instability in the terahertz frequency range. *Phys. Rev. B*, 101(23):235420, 2020.

[13] G.R. Aizin, J. Mikalopas, and M. Shur. Plasmonic instabilities in two-dimensional electron channels of variable width. *Phys. Rev. B*, 101(24):245404, 2020.

[14] S. Zonetti, S. Siaber, J. E. Cunningham, and O. Sydoruk. Scattering-induced amplification of two-dimensional plasmons: Electromagnetic modeling. *J. Appl. Phys.*, 129(22):223103, 2021.

[15] J.-Q. Lu, M. S. Shur, J. L. Hesler, L. Sun, and R. Weikle. Terahertz detector utilizing two-dimensional electronic fluid. *IEEE Electron Device Lett.*, 19(10):373–375, 1998.

[16] W. Knap, Y. Deng, S. Rumyantsev, J.-Q. Lu, M. S. Shur, C. A. Saylor, and L. C. Brunel. Resonant detection of subterahertz radiation by plasma waves in a submicron field-effect transistor. *Appl. Phys. Lett.*, 80(18):3433–3435, 2002.

[17] A. Lisauskas, W. Von Spiegel, S. Boubanga-Tombet, A. El Fatimy, D. Coquillat, F. Teppe, N. Dyakonova, W. Knap, and H. G. Roskos. Terahertz imaging with gaas field-effect transistors. *Electron. Lett.*, 44(6):408–409, 2008.

[18] A. Lisauskas, U. Pfeiffer, E. Öjefors, P. H. Bolìvar, D. Glaab, and H. G. Roskos. Rational design of high-responsivity detectors of terahertz radiation based on distributed self-mixing in silicon field-effect transistors. *J. Appl. Phys.*, 105(11):114511, 2009.

[19] L. Vicarelli, M. S. Vitiello, D. Coquillat, A. Lombardo, A. C. Ferrari, W. Knap, M. Polini, V. Pellegrini, and A. Tredicucci. Graphene field-effect transistors as room-temperature terahertz detectors. *Nat. Mater.*, 11(10):865–871, 2012.

[20] D. A. Bandurin, D. Svintsov, I. Gayduchenko, Sh. G. Xu, A. Principi, M. Moskotin, I. Tretyakov, D. Yagodkin, S. Zhukov, T. Taniguchi, K. Watanabe, I. V. Grigorieva, M. Polini, G. N. Goltsman, A. K. Geim, and G. Fedorov. Resonant terahertz detection using graphene plasmons. *Nat. Commun.*, 9(1):1–8, 2018.

[21] S. J. Allen, D. C. Tsui, and R. A. Logan. Observation of the two-dimensional plasmon in silicon inversion layers. *Phys. Rev. Lett.*, 38:980—983, 1977.

[22] T. N. Theis. Plasmons in inversion layers. *Surf. Sci.*, 98:515–532, 1980.

[23] E. Batke, D. Heitmann, and C. W. Tu. Plasmon and magnetoplasmon excitation in two-dimensional electron space-charge layers on GaAs. *Phys. Rev. B*, 34:6951–6960, 1986.

[24] T. Otsuji, Y. M. Meziani, T. Nishimura, T. Suemitsu, W. Knap, E. Sano, T. Asano, and V. V. Popov. Emission of terahertz radiation from dual grating gate plasmon-resonant emitters fabricated with InGaP/InGaAs/GaAs material systems. *J. Phys.: Condens. Matter*, 20:384206–1–11, 2008.

[25] Y. Yu, Zh. Zheng, H. Qin, J. Sun, Y. Huang, X. Li, Zh. Zhang, D. Wu, Y. Cai, B. Zhang, and V. V. Popov. Observation of terahertz plasmon and plasmon-polariton splitting in a grating-coupled algan/gan heterostructure. *Opt. Express*, 26(24):31794–31807, 2018.

[26] D. Pashnev, T. Kaplas, V. Korotyeyev, V. Janonis, A. Urbanowicz, J. Jorudas, and I. Kašalynas. Terahertz time-domain spectroscopy of two-dimensional plasmons in algan/gan heterostructures. *Appl. Phys. Lett.*, 117(5):051105, 2020.

[27] J. Lusakowski, W. Knap, N. Dyakonova, L. Varani, J. Mateos, T. Gonzalez, Y. Roelens, S. Bollaert, A. Cappy, and K. Karpierz. Voltage tuneable terahertz emission from a ballistic nanometer InGaAs/InAlAs transistor. *J. Appl. Phys.*, 97:064307–1–7, 2005.

[28] G.C. Dyer, G.R. Aizin, J.L. Reno, E.A Shaner, and S.J. Allen. Novel tunable millimeter-wave grating-gated plasmonic detectors. *IEEE J. Sel. Top. Quant. Electron.*, 17:85–91, 2011.

[29] G. C. Dyer, G. R. Aizin, S. J. Allen, A. D. Grine, D. Bethke, J. L. Reno, and E. A. Shaner. Induced transparency by coupling of Tamm and defect states in tunable terahertz plasmonic crystals. *Nat. Photon.*, 7(11):925–930, 11 2013.

[30] A. Di Gaspare, V. Giliberti, E. Giovine, F. Evangelisti, and M. Ortolani. Spectroscopic study of plasma wave resonances of a two-dimensional electron gas in a microcavity at low temperatures. *J. Opt.*, 15:114012–1–6, 2013.

[31] J. B. Wu, A. S. Mayorov, C. D. Wood, D. Mistry, L. H. Li, W. Muchenje, M. C. Rosamond, L. Chen, E. H. Linfield, A. G. Davies, and J. E. Cunningham. Excitation, detection, and electrostatic manipulation of terahertz-frequency range plasmons in a two-dimensional electron system. *Sci. Rep.*, 2015.

[32] J. B. Wu, O. Sydoruk, A. S. Mayorov, C. D. Wood, D. Mistry, L. Li, E. H. Linfield, A. G. Davies, and J. E. Cunningham. Time-domain measurement of terahertz frequency magnetoplasmon resonances in a two-dimensional electron system by the direct injection of picosecond pulsed currents. *Appl. Phys. Lett.*, 108(9):091109, 2016.

[33] S. J Park, S. Zonetti, R. S. Parker-Jervis, J. B. Wu, C. D. Wood, L. H. Li, A. G. Davies, E. H. Linfield, O. Sydoruk, and J. E. Cunningham. Terahertz magnetoplasmon resonances in coupled cavities formed in a gated two-dimensional electron gas. *Opt. Express*, 29(9):12958–12966, 2021.

[34] F. Stern. Polarizability of a two-dimensional electron gas. *Phys. Rev. Lett.*, 18(14):546, 1967.

[35] F. J. Crowne. Contact boundary conditions and the Dyakonov-Shur instability in high electron mobility transistors. *J. Appl. Phys.*, 82:1242–1254, 1997.

[36] O. Sydoruk, R. R. A. Syms, and L. Solymar. Distributed gain in plasmonic reflectors and its use for terahertz generation. *Opt. Express*, 20:19618–19627, 2012.

[37] A. S. Petrov, D. Svintsov, V. Ryzhii, and M. S. Shur. Amplified-reflection plasmon instabilities in grating-gate plasmonic crystals. *Phys. Rev. B*, 95(4), 2017.

[38] M.Ĭ. Dyakonov and M.S̃. Shur. Plasma wave electronics: novel terahertz devices using two dimensional electron fluid. *IEEE Trans. Electron. Dev.*, 43:1640 – 1645, 1996.

[39] V. V. Popov, D. V. Fateev, T. Otsuji, Y. M. Meziani, D. Coquillat, and W. Knap. Plasmonic terahertz detection by a double-grating-gate field-effect transistor structure with an asymmetric unit cell. *Appl. Phys. Lett.*, 99:243504, 2011.

[40] A. L. Fetter. Magnetoplasmons in a two-dimensional electron fluid: Disk geometry. *Phys. Rev. B*, 33(8):5221, 1986.

[41] C. Dahl, S. Manus, J. P. Kotthaus, H. Nickel, and W. Schlapp. Edge magnetoplasmons in single two-dimensional electron disks at microwave frequencies: Determination of the lateral depletion

length. *Appl. Phys. Lett.*, 66(17):2271–2273, 1995.

[42] I. V. Kukushkin, J. H. Smet, S. A. Mikhailov, D. V. Kulakovskii, K. Von Klitzing, and W. Wegscheider. Observation of retardation effects in the spectrum of two-dimensional plasmons. *Phys. Rev. Lett.*, 90(15):156801, 2003.

[43] V. M. Muravev, P. A. Gusikhin, I. V. Andreev, and I. V. Kukushkin. Novel relativistic plasma excitations in a gated two-dimensional electron system. *Phys. Rev. Lett.*, 114(10):106805, 2015.

[44] P. A. Gusikhin, V. M. Muravev, A. A. Zagitova, and I. V. Kukushkin. Drastic reduction of plasmon damping in two-dimensional electron disks. *Phys. Rev. Lett.*, 121:176804, Oct 2018.

[45] O. Sydoruk, R. R. A. Syms, and L. Solymar. Plasma oscillations and terahertz instability in field-effect transistors with Corbino geometry. *Appl. Phys. Lett.*, 97:263504, 2010.

[46] G. R. Aizin, J. Mikalopas, and M. Shur. Current-driven Dyakonov-Shur instability in ballistic nanostructures with a stub. *Phys. Rev. Appl.*, 10(6):064018, 2018.

[47] A. L. Fetter. Edge magnetoplasmons in a bounded two-dimensional electron fluid. *Phys. Rev. B*, 32(12):7676–7684, 1985.

[48] V. A. Volkov and S. A. Mikhailov. Edge magnetoplasmons: low frequency weakly damped excitations in inhomogeneous two-dimensional electron systems. *JETP*, 67(8):1639, 1988.

[49] A. Dawood, J. B. Wu, C. D. Wood, L. H. Li, E. H. Linfield, A. G. Davies, J. E. Cunningham, and O. Sydoruk. Full-wave modelling of terahertz frequency plasmons in two-dimensional electron systems. *J. Phys. D: Appl. Phys.*, 52(21):215101, 2019.